Bioactive Materials 15 (2022) 160–172

Contents lists available at ScienceDirect

Bioactive Materials

journal homepage: www.keaipublishing.com/en/journals/bioactive-materials

DNA-based artificial dendritic cells for in situ cytotoxic T cell stimulation and immunotherapy

Quoc-Viet Le [a,1], Jaiwoo Lee [a,1], Junho Byun [a], Gayong Shim [b,**], Yu-Kyoung Oh [a,*]

[a] College of Pharmacy and Research Institute of Pharmaceutical Sciences, Seoul National University, 1 Gwanak-ro, Gwanak-gu, Seoul, 08826, Republic of Korea
[b] School of Systems Biomedical Science, Soongsil University, Seoul, 06978, Republic of Korea

ARTICLE INFO

Keywords:
Artificial dendritic cell
DNA microflower
In situ T cell stimulation
Programmed T cell expansion
Immunotherapy

ABSTRACT

In immunotherapy, ex vivo stimulation of T cells requires significant resources and effort. Here, we report artificial dendritic cell-mimicking DNA microflowers (DM) for programming T cell stimulation in situ. To mimic dendritic cells, DNA-based artificial dendritic microflowers were constructed, surface-coated with polydopamine, and further modified with anti-CD3 and anti-CD28 antibodies to yield antibody-modified DM (DM-A). The porous structure of DM-A allowed entrapment of the T cell-stimulating cytokine, ineterleukin-2, yielding interleukin-2-loaded DM-A (DM-AI). For comparison, polystyrene microparticles coated with polydopamine and modified with anti-CD3 and anti-CD28 antibodies (PS-A) were used. Compared to PS-A, DM-AI showed significantly greater contact with T cell surfaces. DM-AI provided the highest ex vivo expansion of cytotoxic T cells. Local injection of DM-AI to tumor tissues induced the recruitment of T cells and expansion of cytotoxic T cells in tumor microenvironments. Unlike the other groups, model animals injected with DM-AI did not exhibit growth of primary tumors. Treatment of mice with DM-AI also protected against growth of a rechallenged distant tumor, and thus prevented tumor recurrence in this model. DM-AI has great potential for programmed stimulation of $CD8^+$ T cells. This concept could be broadly extended for the programming of specific T cell stimulation profiles.

1. Introduction

T cells play crucial roles in various immune diseases and immunotherapies. The expansion of T cells to specific T cell types may govern the efficacy of immunotherapy. In cancer immunotherapy, the populations of cytotoxic T cells ($CD8^+$ T cells) play indispensable roles in scavenging and killing tumor cells [1]. In addition, the ratio of $CD8^+$ T cells to regulatory T (Treg) cells has been shown to correlate with clinical cancer immunotherapy outcomes [2,3]. An imbalance of $CD8^+$ T cells versus Treg cells may lead to the outgrowth of tumor tissues [4]. Thus, it would be clinically important to modulate the tumor immune microenvironment to direct the expansion of cytotoxic T cells.

To date, limited approaches have been used to stimulate T cells. For such purposes, microparticles are typically preferred over nanoparticles due to the former having larger contact areas with T cells [5,6]. In ex vivo studies, polymeric microparticles have been modified with stimulating cocktails of antibodies and co-cultured with T cells [7–9]. Efforts have been made to construct ellipsoid polymeric nanoparticles that exhibit improved contact with T cells [8,10]. However, most existing studies have used microparticles with smooth surfaces.

In this study, we designed dendritic cell-inspired DNA microflowers for directed T cell stimulation (Fig. 1). We employed the dendritic topology of DNA microflowers with multiple leaflet structures. To stimulate the expansion of T cells, the DNA microflower structures were modified with anti-CD3 and anti-CD28 antibodies. To further direct the expansion of T cells to $CD8^+$ T cells, the porous structures of the DNA microflowers were loaded with the cytokine, human interleukin 2 (hIL2). Here, we report the stimulation and $CD8^+$T cell-directed expansion effects of artificial antibody-coated dendritic cell-mimetic DNA microflowers loaded with hIL2 (DM-AI). We show that the intratumoral administration of DM-AI could provide immunotherapeutic effects against primary and distant tumors in a mouse model. Although we demonstrate the use of DM-AI for $CD8^+$ T cell-directed stimulation, the concept may be broadly applied for treatment of various

Peer review under responsibility of KeAi Communications Co., Ltd.
* Corresponding author.
** Corresponding author.
E-mail addresses: shim@ssu.ac.kr (G. Shim), ohyk@snu.ac.kr (Y.-K. Oh).
[1] These authors made equal contributions to this work.

https://doi.org/10.1016/j.bioactmat.2021.12.001
Received 21 August 2021; Received in revised form 3 December 2021; Accepted 13 December 2021
Available online 23 December 2021

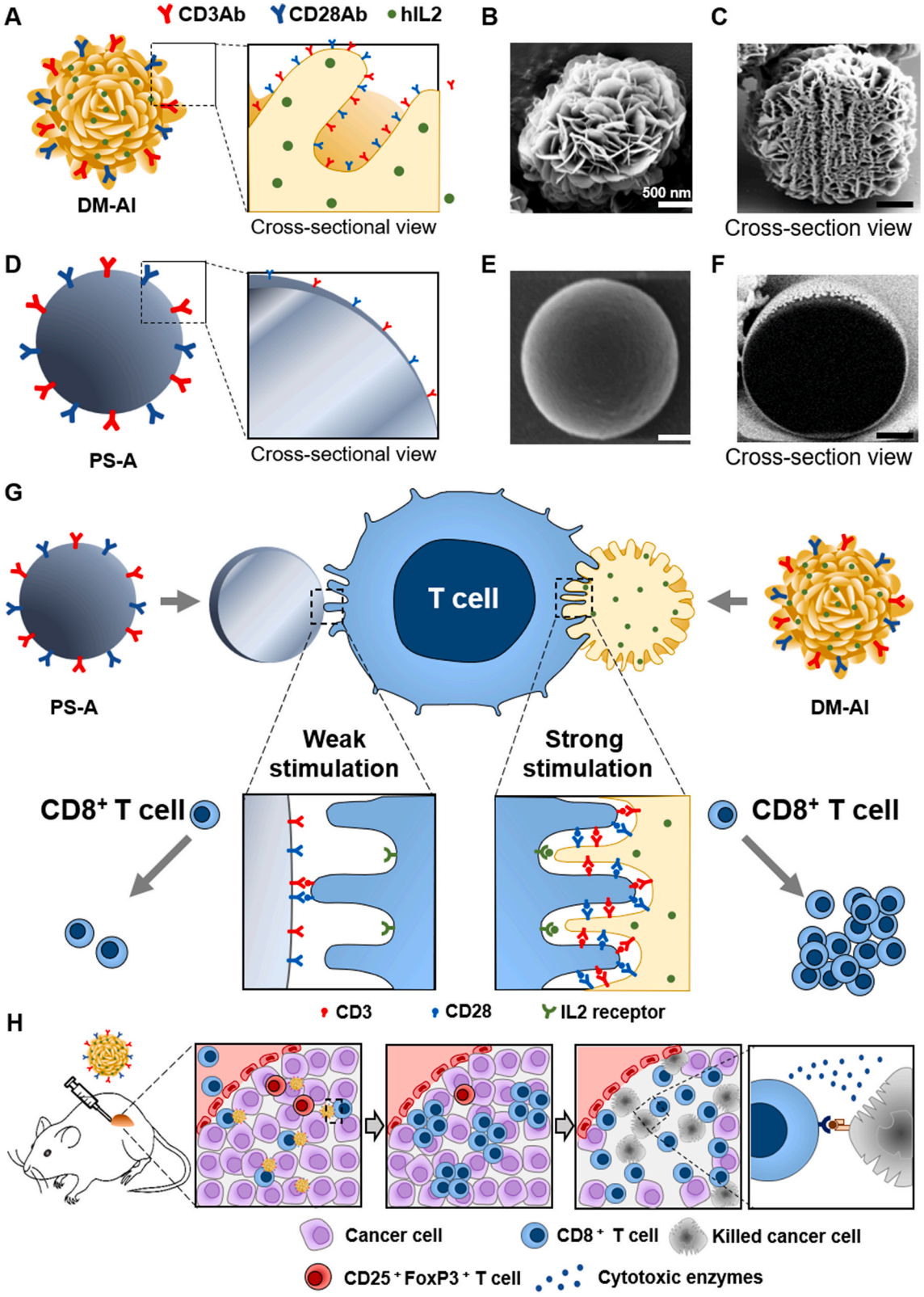

Fig. 1. Schematic illustration of DM-AI and proposed mechanism. (A) Illustration of DM-AI structure. DM was synthesized by rolling-circle amplification and coated with PDA. Two T cell-stimulating signals (anti-CD3 and anti-CD28 antibodies) were conjugated onto the DM surface, and a third T cell-stimulating signal (hIL2) was entrapped in the porous cavity of the microflower structure to yield DM-AI. (B) SEM picture of DM-AI. (C) Cross section of DM-AI observed by SEM. (D) For comparison, PS microparticles were coated with PDA and modified with anti-CD3 and anti-CD28 antibodies. (E) SEM picture of PS-A. (F) Cross section of PS-A observed by SEM. (G) Proposed action mechanism of DM-AI in T cell interaction and activation. Dendritic cell-like DM-AI particles have ruffled surfaces, allowing the stimulating antibodies to closely interact with $CD8^+$ T cells. Compared with smooth-surfaced PS-A, DM-AI provides a larger contact area to yield higher $CD8^+$ T cell activation. (H) In vivo local administration of DM-AI is proposed to expand the populations of $CD8^+$ T cells and thereby exert immunotherapeutic effects.

immunological diseases.

2. Methods

2.1. Preparation of DNA microflower structures

DNA microflower structures were prepared by rolling-circle amplification (RCA) with a DNA template. To generate the pre-circular RCA template prior to the RCA reaction, 0.5 mM of DNA template (ATCTGACTAGTATATACAAAACTAATGAGGCGTTGGAAGTGT AGTGGGGGCGG TGCGCTCGGTCATAGTAAT; Macrogen Inc., Daejeon, Republic of Korea) was annealed with 0.5 mM of the corresponding primer (5′-TATATACTAGTCAGATATTACT-3'; Macrogen Inc.) in hybridization buffer (1 mM EDTA, 10 mM Tris HCl, 100 mM NaCl, pH 8.0). This pre-circular RCA template was reacted with T4 DNA ligase (125 units/ml; Thermo Scientific, Waltham, MA, USA) for 12 h at 4 °C to close the nick. The resulting circular templates was incubated with phi29 DNA polymerase (100 units/ml; Thermo Scientific) and 2 mM dNTPs (ELPIS-Biotech. Inc., Daejeon, Republic of Korea) for 48 h at 30 °C. The collected RCA products were heated for 10 min at 70 °C for inactivation of phi29 DNA polymerase. After centrifugation at 8000×*g* for 5 min, the obtained pellet was washed three times (8000×*g*, 3 min each) with triple distilled water (TDW). The final DNA microflower pellet was resuspended in TDW and stored at 4 °C until use.

2.2. Immobilization of antibodies

Antibodies were immobilized onto the surfaces of the DNA microflower structures. For conjugation with antibodies, the DNA microflowers were first coated with PDA: Briefly, 2×10^7 DNA microflowers were dispersed in 1 ml of 10 mM Tris buffer (pH 9.2) and mixed with 3 μl of 10 mg/ml dopamine hydrochloride (Sigma-Aldrich). The PDA-coated DNA microflowers (DM) were washed three times by centrifugation with Tris buffer at 4000×*g* for 3 min each. For surface conjugation of antibodies, the DNA microflowers were reconstituted in 50 μl of Tris buffer containing 50 μg/ml anti-CD3e mouse IgG antibody (Cat. No. BE0001-1, Lot No. 703419A1; Bio X Cell, West Lebanon, NH, USA) and 100 μg/ml anti-CD28 mouse IgG antibody (Cat. No. BE0015-1, Lot No. 639918N1; Bio X Cell) and incubated at room temperature for 12 h. The resulting antibody-modified DNA microflower (DM-A) was purified three times by centrifugation with Tris buffer at 4000×*g* for 3 min, and then reconstituted with 100 μl TDW and stored at 4 °C for further use.

For comparison, we prepared antibody-conjugated polystyrene microparticles (PS-A) using commercial polystyrene microparticles (Sigma-Aldrich). In brief, 2×10^7 PS particles were dispersed in 1 ml of 10 mM Tris buffer (pH 9.2) and mixed with 3 μl of 10 mg/ml dopamine hydrochloride. The resulting PDA-coated PS was washed three times by centrifugation at 4000×*g* for 3 min, reconstituted in 50 μl of Tris buffer containing 50 μg/ml anti-CD3e mouse IgG and 100 μg/ml anti-CD28 mouse IgG, and incubated at room temperature for 12 h. The resulting PS-A was purified three times by centrifugation with Tris buffer at 4000×*g* for 3 min, reconstituted with 100 μl TDW, and stored at 4 °C for further use.

The amounts of anti-CD3e antibody and anti-CD28 antibody were quantified by ELISA: The anti-CD3e mouse IgG antibody was quantified using an Armenian hamster IgG ELISA kit (Cat. No. IHMARIGGKT, Innovative research, MI, USA) and the anti-CD28 mouse IgG antibody was quantified using a hamster IgG ELISA kit (Cat. No. ab200010, Abcam, Cambridge, UK).

2.3. Loading of human interleukin 2 to DM-AI

Human interleukin 2 (hIL2) was loaded to DM-AI via complexation with poly-L-lysine (PLL). First, 2 μg of hIL2 (BioLegend, San Diego, CA, USA) was added to 100 of 2×10^7 DM-A and vortexed for 10 s. In experiments involving visualization of hIL2 loading by confocal microscopy, Alexa Fluor™ 680 (Thermo Fisher Scientific)-labeled hIL2 was used. Two microliters of PLL (1 mg/ml; Sigma-Aldrich) in water was added to the mixture of hIL2 and DM-A, followed by sonication for 10 s. After incubation for 12 h at 4 °C, hIL2-loaded DM-A (DM-AI) was washed with TDW by centrifugation. The pelleted DM-AI was reconstituted in 5% glucose and stored at 4 °C until use. The amount of hIL2 loaded in DM-AI was quantified using a human IL2 ELISA kit (R&D Systems, Minneapolis, MN, USA).

2.4. Physicochemical characterization studies

Size, zeta potential, and morphology were characterized for the various samples. The particle size was assessed using the dynamic light scattering method. The zeta potentials of particles were measured by laser Doppler microelectrophoresis at an angle of 22°. Size and zeta potential measurements were performed using an ELS8000 instrument (Photal, Osaka, Japan).

The morphologies of PS-A, DM, DM-A, and DM-AI were visualized using a scanning electron microscope (SEM). The internal microstructures of the microparticles were characterized by assessing cross sections, which were obtained using a focused ion beam field emission scanning electron microscope (FIB-SEM).

The presence of antibodies and hIL2 in particles was visualized using confocal imaging. First, particles were stained for 1 h with FITC-conjugated anti-Syrian hamster antibody (dilution 1:100; BioLegend) and AlexaFluor 594-conjugated anti-Armenian hamster antibody (dilution 1:100; BioLegend). The particles were then stained with 10 μg/ml Hoechst (Sigma-Aldrich) in PBS for 30 min, washed with PBS, and mounted on polyamine-coated coverslips for confocal imaging.

The release of hIL2 from DM-AI was examined in serum and PBS. DM-AI was added to serum or PBS and incubated at 37 °C. At various time points, aliquots (0.1 mL) were collected, and centrifuged at 8000×*g* for 5 min. The supernatant was collected and the amount of released hIL2 was measured using a human IL2 ELISA kit (R&D Systems) following the manufacturer's instructions.

2.5. Animals

Five-week-old Balb/c mice were purchased from Raon Bio (Yongin, Republic of Korea) and housed under standard pathogen-free conditions at the Animal Center for Pharmaceutical Research, Seoul National University. All animal experiments were performed in accordance with the guidelines for the Care and Use of Laboratory Animals of the Institute of Laboratory Animal Resources, Seoul National University (approval number, SNU-190821-5).

2.6. Visualization of T cells and particle interactions

The interactions of T cells with particles were visualized by SEM and confocal microscopy. $CD8^+$ T cells were isolated from splenocytes of Balb/c mice by the negative selection method using a mouse $CD8a^+$ T Cell Isolation Kit (Miltenyi Biotec, Bergisch Gladbach, Germany) and a mouse MojoSort $CD4a^+$ T Cell Isolation Kit (BioLegend). T cells (4×10^5) were seeded to a 96-well plate in complete RPMI. PS-A or DM-AI (8×10^5) was added to each well and incubated overnight. For the positive control group, Dynabeads (Thermo Fisher Scientific) were applied to T cells according to the manufacturer's protocol. Mixtures of T cells and particles were collected by centrifugal wash with pre-warmed PBS (3000×*g*, 5 min).

For SEM imaging, the mixtures of T cells and particles were mounted on PLL-coated coverslips (Neuvitro Corporation, Camas, WA, USA) for 15 min and fixed with pre-warmed Karnovsky fixative solution for 2 h. The mounted T cells and particles were rinsed three times with 50 mM cacodylate buffer and stained with 1% OsO4 solution (500 μl) for 1 h at 4 °C. Each coverslip was dehydrated with a series of ethanol solutions (50, 70, 90, 100%). The dried T cell-particles mixtures were sputter-

coated with 1.5 nm gold-palladium and subjected to SEM imaging using a field-emission scanning electron microscope (Supra 55VP; Carl Zeiss, Oberkochen, Germany). Elemental mapping was conducted by SEM with energy-dispersive X-ray spectroscopy (EDS-SEM).

For confocal imaging, the T cell-particle mixtures were stained with FITC-conjugated anti-Syrian hamster antibody (dilution 1:100; BioLegend), AlexaFluor 594-conjugated anti-Armenian hamster (dilution 1:100; BioLegend) and AlexaFluor 647-conjugated anti-CD8 antibody (BioLegend) and AlexaFluor 647-conjugated anti-CD4 antibody (BioLegend). The T cell-particle mixtures were mounted on PLL-coated coverslips (Neuvitro Corporation), fixed with 4% paraformaldehyde, and counterstained with Hoechst dye (Sigma-Aldrich). The binding of T cells and particles was observed using an SP8 confocal laser microscope (Leica Microsystems, Wetzlar, Germany).

2.7. In vitro T cell activation

Activation of T cells was tested via assessment of proliferation rate and cytokine secretion. T cells were isolated from splenocytes of Balb/c mice using a nylon column as previously described [11]. For activation testing, 4×10^5 T cells/well were plated to a 96-well plate in complete RPMI, treated with PS-A or DM-AI (8×10^5 particles/well), and incubated for 4 days. For comparison, T cells were treated with a mixture of PS-A and 2 ng/ml hIL2 (PS-A + hIL2). After 48 h, the cell culture medium was changed every day.

In some cases, the cytokine-inducing effect of DM-AI (8×10^5 particles/well) was compared with that of 5-fold higher PS-A (40×10^5 particles/well). For quantitation of secreted cytokines, supernatants of activated T cells were collected after 48 h of particle treatment. Secreted IL2 and interferon-γ (IFN-γ) were quantified using mouse IL2 and IFN-γ ELISA kids (R&D Systems), respectively, according to the manufacturer's protocols.

For the proliferation assay, T cells were stained with carboxyfluorescein succinimidyl ester (CFSE, BioLegend) following the manufacturer's protocol. After 4 days of activation, the T cells were collected and stained with phycoerythrin (PE)-conjugated anti-mouse CD4 antibody (dilution 1:100, Cat. No. 100408, Lot No. B266388; BioLegend), Percp-Cy5.5-conjugated anti-mouse CD8 antibody (dilution 1:100, Cat. No. 100734, Lot No. B289962; BioLegend), and APC-conjugated anti-mouse CD3 antibody (dilution 1:100, Cat. No. 100236, Lot No. B288206; BioLegend). The stained T cells were then analyzed using a FACSCalibur flow cytometer (BD Biosciences, CA, USA). The proliferations of $CD3^+CD4^+$ T cell and $CD3^+CD8^+$ cells were assessed based on CFSE signal dilution. The proliferation index of T cells was calculated using FlowJo software (BD Biosciences).

For Treg cell quantification, activated T cells were collected and stained with FITC-conjugated anti-mouse CD25 antibody (dilution 1:100, Cat. No. 102006, Lot No. B252569; BioLegend) and PE-conjugated anti-mouse CD4 antibody (dilution 1:100; BioLegend). The T cells were then fixed, permeabilized with an intracellular staining kit (BioLegend), and subjected to intracellular staining with an APC-conjugated anti-mouse FoxP3 antibody (dilution factor 1:100, Cat. No. 17-5773-82, Lot No. 2062640; Invitrogen). The stained cells were analyzed using a FACSCalibur flow cytometer. The Treg cells were gated as $CD4^+$CD25+FoxP3+ T cells and the percentage of Treg cells was analyzed using FlowJo software.

T cell subsets were identified by measuring the expression levels of IFN-γ and IL4 using flow cytometry and ELISA kits. Activated T cells were collected and stained with FITC-conjugated anti-mouse CD3 antibody (dilution 1:100, Cat. No. 100204, Lot No. B336473; BioLegend) and APC/Cy7-conjugated anti-mouse CD4 antibody (dilution 1:100; Cat. No. 100414, Lot No. B326190; BioLegend). The T cells were then fixed, permeabilized with an intracellular staining kit (BioLegend), and subjected to intracellular staining with a BV421-conjugated anti-mouse IFN-γ antibody (dilution 1:50, Cat. No. 505830, Lot No. B335329; BioLegend) and a PE-conjugated anti-mouse IL4 antibody (dilution 1:50, Cat. No. 504104, Lot No. B271497; BioLegend). The stained cells were analyzed using a BD LSR Fortessa X-20 flow cytometer (BD Bioscience). Th1 cells were gated as $CD3^+CD4^+$ IFN-γ+ T cells and Th2 cells were gated as $CD3^+CD4^+$ IL4+ T cells. The percentage of Th1/Th2 cells was analyzed using FlowJo software.

For the identification of T cell subsets by secreted cytokines, $CD4^+$ T cells were isolated by a mouse MojoSort CD4a + T Cell Isolation Kit (BioLegend) and treated with microparticles. Two days later, the levels of IFN-γ and IL4 in the supernatants were quantified using mouse IFN-γ (Cat. No. DY485, R&D Systems) and IL4 (No. DY404, R&D Systems) ELISA kits, respectively.

2.8. In vitro study of the anti-cancer effects of activated T cells

The in vitro anticancer effects of our formulations were examined using a co-culture model comprising cancer-reactive T cells and cancer cells. Total T cells were isolated from the splenocytes of mice that had been immunized with CT26 cancer cell lysates and imiquimod, as previously reported with slight modification [12]. Briefly, Balb/c mice were injected intraperitoneally with 100 μg CT26 protein lysate mixed with 100 μg imiquimod once per week for 3 weeks. Seven days after the last immunization, mice were euthanized and splenocytes were isolated. Total T cells were obtained from the splenocytes using a nylon column. For activation, 4×10^5 T cells/well in a 96-well plate were treated with PS-A or DM-AI (8×10^5/well) and incubated for 4 days. The T cells were then washed twice with PBS and resuspended with complete RPMI supplemented with 30 U/ml IL2. CT-26 cells stained with Calcein-AM (Thermo Fisher Scientific) were added to each well (4×10^4 cells/-well), and the plate was incubated 24 h for co-culture. As a negative control, cell culture medium was used. As a positive control, 0.1% saponin was used to induce complete lysis of the cancer cells. The cancer cell lysis-induced release of Calcein AM to the supernatant was monitored to evaluate the cancer cell-killing effects of the activated T cells. Supernatants were collected and fluorescence intensity was measured at 485 nm excitation and 535 nm emission using a Multireader SpectraMAX M5 (Molecular Devices, San Joe, CA, USA). The cancer cell viability was calculated from the fluorescence intensity of each groups normalized with respect to the positive and negative controls.

2.9. In vivo study of immunotherapeutic effects and biodistribution

In vivo immunotherapeutic effects were assessed using primary and distant syngeneic tumor models. Six-week-old Balb/c mice were first inoculated with 1×10^6 CT26 cells on the right flank as the primary tumor. Seven days after primary tumor inoculation, the mice were inoculated with 3×10^5 CT26 cells on the left flank as the distant tumor, and locally injected with 50 μl of 2×10^7 particles (PS-A, DM-A, DM-A + hIL2, or DM-AI) at the primary tumor site. To induce inflammation at tumor tissues, at 5 min after the injection of particles, the tumor site was irradiated with NIR laser light (BWT Beijing, Beijing, China) at an output power of 1.5 W for 15 min. The tumor temperature was monitored using an infrared thermal imaging system (FLIR T420; FLIR System Inc., Danderyd, Sweden). Thereafter, particles were injected intratumorally at 3-day intervals for three more repeated doses. The volumes of the primary and distant tumors were monitored every 2–3 days. Tumor volume was calculated using the equation $a \times b^2 \times 0.5$, where a is the largest dimension and b is the smallest dimension [13].

The biodistribution of DM-AI was determined by molecular imaging. For imaging, Cy5 dCTP (GEPA55021, Sigma-Aldrich) was used to synthesize fluorescent Cy5-labeled DM-AI. The resulting Cy5-DM-AI was intratumorally injected (2×10^7 particles in 50 μl) at 7 days after tumor inoculation. The fluorescence intensities of the whole body, tumor tissues, and major organs were assessed using an In Vivo Imaging System (IVIS; PerkinElmer, Hopkinton, MA, USA) at several time points.

2.10. Characterization and quantification of tumor-infiltrating T cells in tumor tissues

Tumor-infiltrating lymphocytes were profiled by flow cytometry. Seven days after the first injection of particles, mice were euthanized and tumor tissues were isolated. The collected tissues were minced into small pieces using scissors and digested with RPMI medium supplemented 1 mg/ml collagenase (Sigma-Aldrich). The obtained tumor cell suspension was washed with 2% FBS/PBS and filtered through a 40-μm cell strainer to obtain a single-cell suspension.

For quantification of $CD4^+$ and $CD8^+$ T cells, the tumor cell suspension was stained with PE-conjugated anti-mouse CD4 antibody (dilution 1:100; BioLegend), Percp-Cy5.5-conjugated anti-mouse CD8 antibody (dilution 1:100; BioLegend), and APC-conjugated anti-mouse CD3 antibody (dilution 1:100; BioLegend). The stained tumor cells were then analyzed using a FACSCalibur flow cytometer. The percentage of $CD3^+CD4^+$ T cells and $CD3^+CD8^+$ T cells were analyzed using FlowJo software.

To assess the Granzyme B activity of $CD8^+$ T cells in tumor tissues, the tumor cell suspension was stained with FITC-conjugated anti-mouse CD3 antibody (dilution 1:100; BioLegend) and Percp-Cy5.5-conjugated anti-mouse CD8 antibody. The T cells were then fixed and permeabilized with an intracellular staining kit (BioLegend) and intracellularly stained with AlexaFluor 647-conjugated anti-mouse Granzyme B antibody (dilution 1:100, Cat. No. 515406, Lot No. B233111; BioLegend). The $CD8^+GrzB^+$ cells were sorted by flow cytometry and analyzed using FlowJo software.

To evaluate the Treg cell population in tumor tissues, the tumor cell suspension was surface stained with FITC-conjugated anti-mouse CD25 antibody (dilution 1:100; BioLegend) and PE-conjugated anti-mouse CD4 antibody (dilution 1:100; BioLegend) and intracellularly stained with APC-conjugated anti-mouse FoxP3 antibody. The Treg cells were gated as $CD4^+CD25^+FoxP3^+$ T cells and the percentage of Treg cells was analyzed using FlowJo software.

2.11. Statistical analysis

The experimental data were analyzed by two-sided analysis of variance (ANOVA) with Dunnett's post-hoc test. All statistical analyses were carried out using Prism (version 7.0; GraphPad Software, San Diego, CA, USA). The comparison was considered to reach statistical significance when P was less than 0.05.

3. Results

3.1. Characterization of DM-AI

DM-AI was characterized for its size, net charge, morphology, and the existence of T cell-stimulating signals. The proposed structures of DM-AI and PS-A are shown in Fig. 1A and C, respectively. In the cross-sectional view, DM-AI had a dendritic surface and an internal porous network (Fig. 1C), whereas PS-A showed a spherical shape and a solid

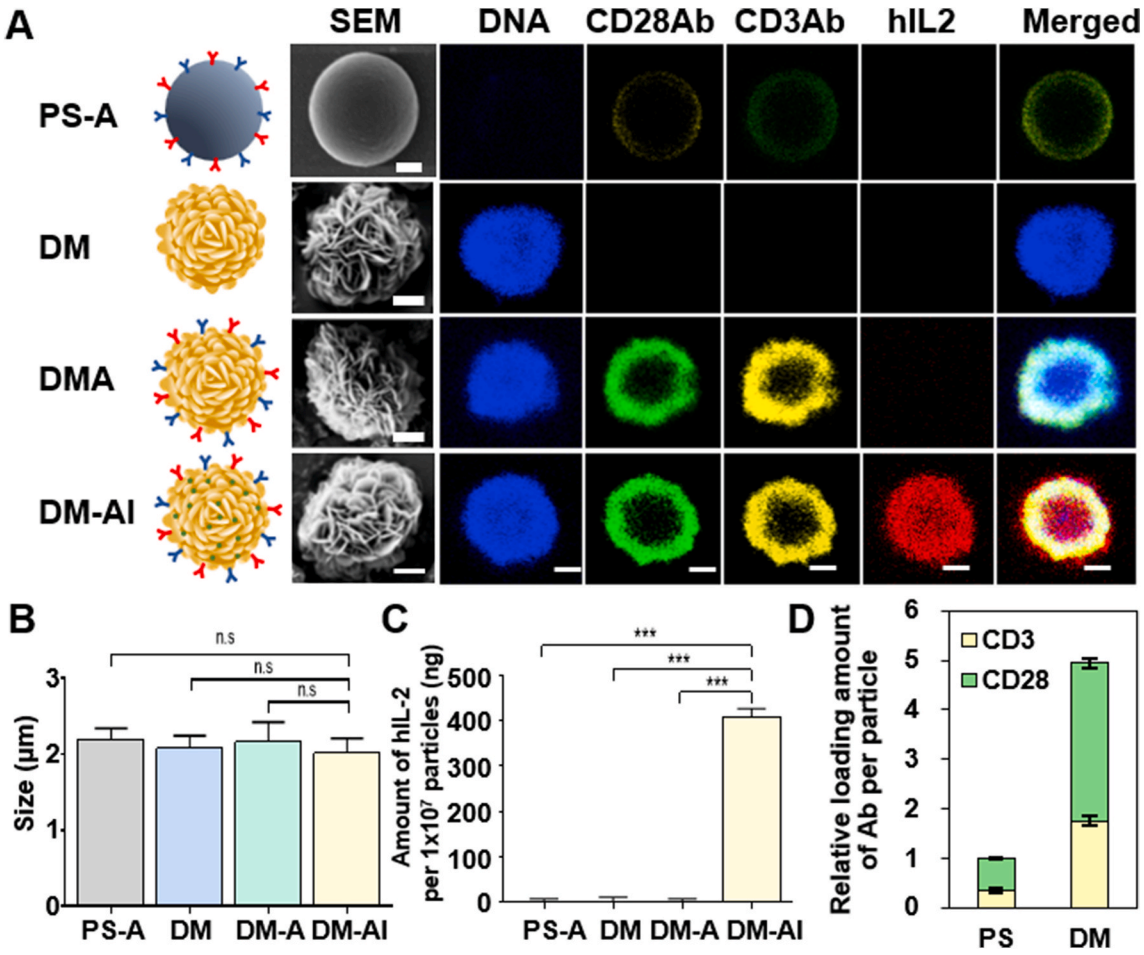

Fig. 2. Characterization of microparticles. (A) For the various particles, SEM images and confocal fluorescence images were obtained for DNA, anti-CD28 antibody (CD28Ab), anti-CD3 antibody (CD3Ab), and hIL2 staining. Scale bar: 0.5 μm. (B) Sizes of microparticles were measured by dynamic light scattering. (C, D) Loading amount of hIL2 (C) and anti-CD3 and anti-CD28 antibodies (D) in each sample was measured by ELISA. ***: significantly different from the other groups at $P < 0.001$; n.s.: not significantly different ($P > 0.05$).

core (Fig. 1F). SEM images showed that DM, DM-A, and DM-AI had flower-like shapes (Fig. 2A). The fluorescence signal corresponding to DNA was observed in DM, DM-A, and DM-AI, but not in PS-A (Fig. 2A). The anti-CD28 antibody (external), anti-CD3 antibody (external), and hIL2 (internal) were present in DM-AI (Fig. 2A). The average size of DM-AI was 1.83 ± 0.17 μm, which was not significantly different from that of the other microparticles (Fig. 2B).

The loading amount of the two antibodies was 4.9 times higher for DM than for PS (Fig. 2D). The anti-CD3 and anti-CD28 antibodies were loaded onto DM at amounts of 0.91 ± 0.05 μg/10^7 particles and 1.64 ± 0.05 μg/1 × 10^7 particles, respectively. The loading weight ratio of anti-CD3 versus anti-CD28 antibody on DM was 1:1.80. The anti-CD3 and anti-CD28 antibodies were loaded onto PS at amounts of 0.18 ± 0.01 μg/10^7 particles and 0.34 ± 0.03 μg/10^7 particles, respectively. The content of hIL2 loaded to DM-AI was 409 ± 17.8 ng per 1 × 10^7 particles (Fig. 2C). The release kinetics of hIL2 from DM-AI were tested in serum and PBS (Fig. S1). When incubated in PBS, DM-AI did not show the release of hIL2. In contrast, the incubation of DM-AI in serum showed time-dependent release of hIL2. The release of hIL2 was sustained over 3 days.

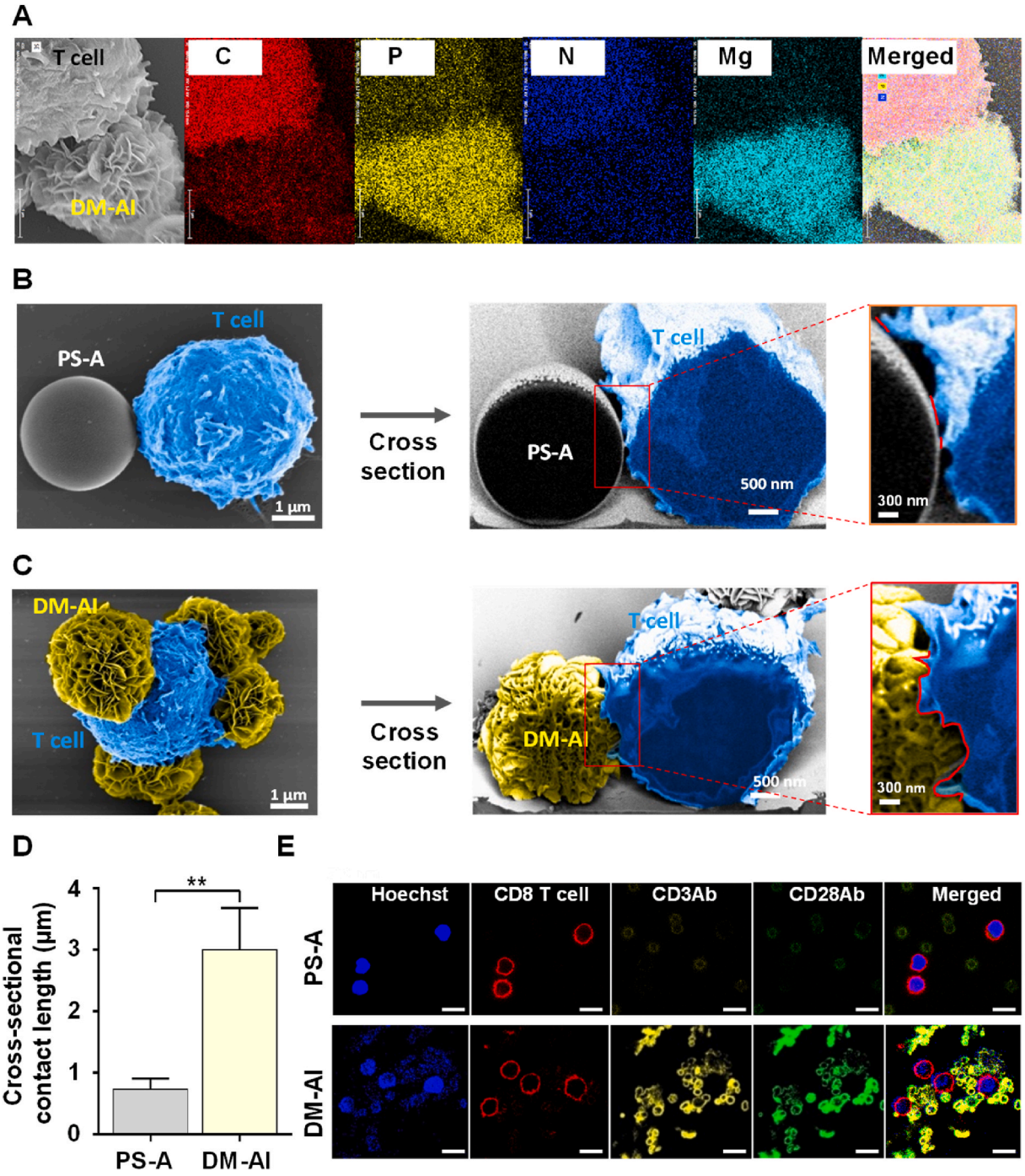

Fig. 3. Interaction of T cells with microparticles. (A) EDS-SEM elemental mapping images of T cells interacting with DM-AI (C, carbon; N, nitrogen; P, phosphorous; Mg, magnesium). (B, C) Surface-scanning and cross-sectional images of T cells bound with PS-A (B) or DM-AI (C). (D) The contact lengths of T cells with particles were measured by image analysis. **: significantly different at $P < 0.01$. (E) Confocal microscopic images of $CD8^+$ T cells co-cultured with PS-A or DM-AI (Hoechst, nuclei of T cells; CD8 T cell, CD8-positive T cells; CD3Ab, anti-CD3 antibody on particles; CD28Ab, anti-CD28 antibody on particles). Scale bar: 4 μm.

3.2. Interaction of DM-AI and T cells

The interactions of T cells with microparticles were visualized by SEM and confocal microscopic imaging. EDS-SEM element mapping (Fig. 3A) and energy-dispersive spectrum analysis (Fig. S2) shows that T cells higher in carbon and nitrogen closely interact with DM-AI microparticles rich with phosphorus and magnesium.

Comparison of cross-sections revealed that PS-A and DM-AI had different contact areas: PS-A showed a few discrete contact loci with T cells (Fig. 3B), whereas DM-AI showed continuous contact areas (Fig. 3C). Image analysis revealed that DM-AI had a 4.1-fold greater contact length with T cells compared to PS-A (Fig. 3D). Confocal imaging of T cells and microparticles in co-culture showed that a single $CD8^+$ T cell was unlikely to interact with PS-A, but was likely to be surrounded by several DM-AI particles (Fig. 3E). DM-AI also showed a higher interaction with $CD4^+$ T cells, compared to that of PS-A (Fig. S3).

3.3. In vitro expansion of T cells

We observed that the stimulation of T cells by DM-AI depended on the ratio of cell number to particle number (Fig. S4). The optimal activity of DM-AI was observed when the ratio of T cells to DM-AI particles was 1:2: Using a ratio of 1:2 yielded a higher expansion of T cells than using a 1:1 ratio, but further increasing the ratio to 1:4 did not significantly increase the expansion of T cells. Thus, a T cell to DM-AI ratio of 1:2 was used for further experiments.

Upon co-culture with T cells, DM-AI significantly promoted greater stimulation of T cells to $CD8^+$ T cells compared to the other studied particles. Compared to the untreated group, PS-A, DM-A, and DM-AI showed higher proliferation of T cells to $CD4^+$ and $CD8^+$ T cells (Fig. 4A). The expansion index values revealed that the expansion from T cells to $CD8^+$ T cells was the highest in the group treated with DM-AI, which showed 1.5- and 4.1-fold higher values compared to DM-A and PS-A, respectively (Fig. 4B).

Notably, the co-culture of T cells with DM-derived particles affected the propagation to Treg cells. Compared to PS-A, DM-A and DM-AI triggered significantly less differentiation of T cells to Treg cells (Fig. 4C and D). Although DM-A and DM-AI triggered similar levels of Treg differentiation, DM-AI induced greater secretion of cytokines from T cells. In T cells treated with DM-AI, the secretion levels of IL2 (Fig. 4E) and IFN-γ (Fig. 4F) were 3.4- and 1.8-fold higher than those in the group treated with DM-A. Moreover, T helper cells stimulated by DM-AI differentiated to Th1 cells with Th1-dominant cytokine secretion patterns (Figs. S5A–5F). The Th1/Th2 ratio was significantly higher in the DM-AI group compared to the other groups (Fig. S5G). The Th1/Th2 ratio of the DM-AI-treated group was 3.3- and 4.2-fold higher than those of the groups treated with PS-A + hIL2 and PS-A, respectively.

We also tested whether the higher T cell stimulatory effect of DM-AI over PS-A was proportional to the 4.9-fold higher amounts of antibodies. However, treatment of T cells with 5-fold higher numbers of PS-A or PS-A plus hIL2 still yielded significantly lower secretion of IL2 and IFN-γ, compared to DM-AI treatment (Fig. S6). To test the role of hIL2 in T cell activation by PS-based particles, we treated T cells with a physical mixture of PS-A and hIL2 (Fig. S7) and observed expansion. The expansions of $CD3^+CD4^+$ T cells and $CD3^+CD8^+$ T cells were 1.76- and 3.27-fold higher, respectively, in the DM-AI group compared to the PS-A + hIL2 group.

3.4. Anticancer effects of stimulated T cells

The ex vivo anticancer effects of stimulated T cells were studied as illustrated in Fig. 5A. T cells were treated with various microparticles

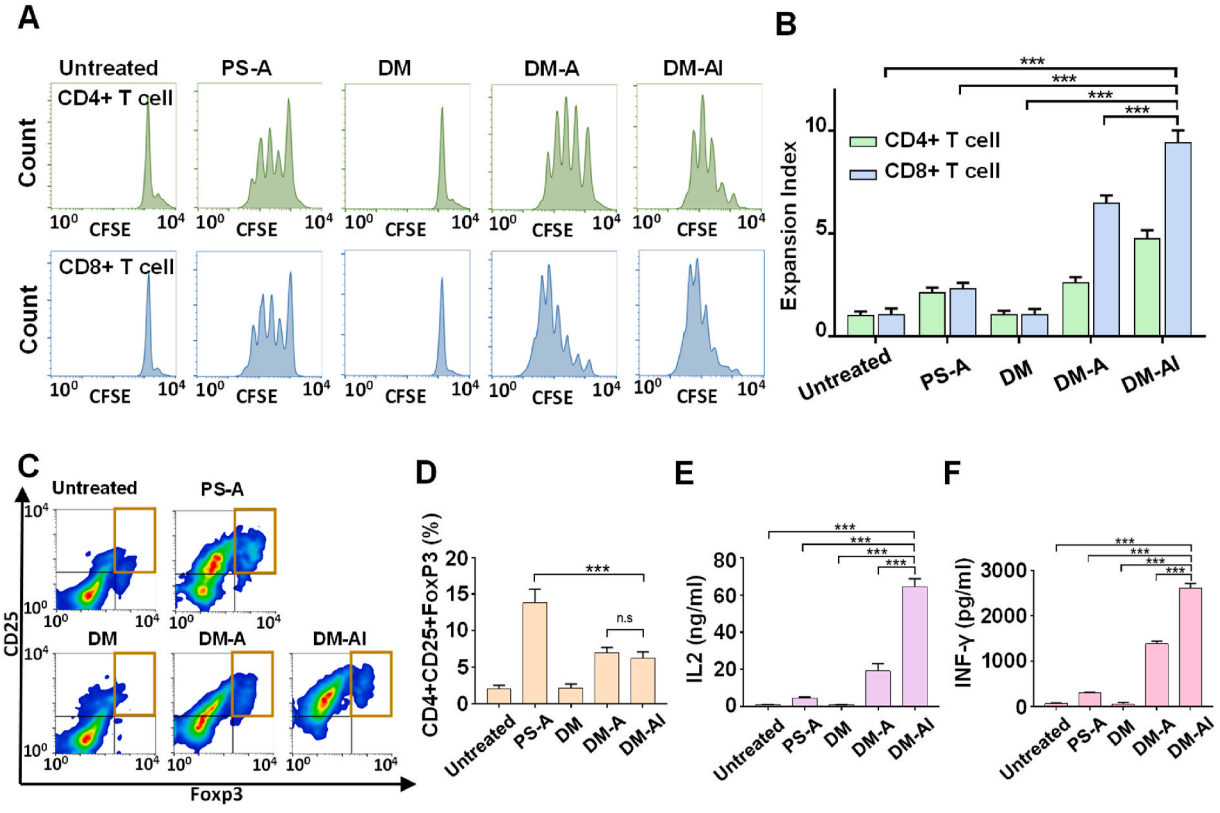

Fig. 4. In vitro T cell activation by DM-AI. (A) Naïve T cells were stained with CFSE dye and proliferation was examined 4 days after treatments with various particles. $CD3^+CD8^+$ T cells and $CD3^+CD4^+$ T cells were gated for CFSE signal analysis. (B) The fold expansion of each T cell population was measured by CFSE assay. (C) Treg cell differentiation was analyzed as the population of $CD4^+CD25^+FoxP3^+$. (D) The ratio of Treg cells to total CD4 T cells. (E, F) Supernatants of T cells treated with the various formulations were analyzed for IL2 (E) and IFN-γ (F). ***: significantly different at $P < 0.001$; n.s.: not significantly different ($P > 0.05$).

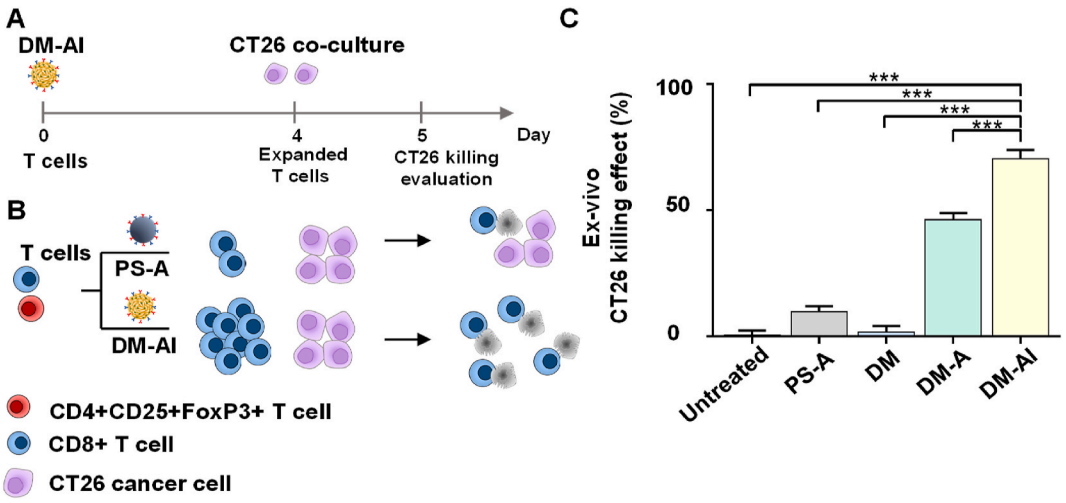

Fig. 5. In vitro anti-cancer effect by DM-AI. (A) T cells were treated with various microparticles for 4 days and co-cultured with CT26 tumor cells. At day 5, the ex vivo killing of tumor cells was monitored. (B) Illustration of the ex vivo study scheme. Anti-tumor-specific T cell pools were collected from splenocytes of CT26 tumor lysate-immunized mice. Each T cell pool was expanded with the various samples and all expanded T cells were co-cultured with CT26 cells. (C) Ex vivo killing effects were determined by the percentage of dead cancer cells observed after co-culture with T cells. ***: significantly different at $P < 0.001$.

and co-cultured with CT26 tumor cells. The stimulation of T cells to $CD8^+$ T cells by DM-AI appeared to effectively kill the co-cultured CT26 tumor cells (Fig. 5B). The ex vivo killing effect of CT26 tumor cells was highest in the DM-AI-treated group, followed by the DM-A, PS-A, and DM groups (Fig. 5C). The ex vivo CT26 tumor cell killing effect was 1.5- and 7.2-fold higher in the DM-AI-treated group compared to the DM-A- and PS-A-treated groups, respectively.

3.5. *In vivo anticancer efficacy*

The biodistribution of DM-AI was observed using fluorescent Cy5-tagged Cy5-DM-AI. Whole-body imaging (Fig. 6A) and ex vivo imaging (Fig. 6B) revealed that the fluorescence signal of DM-AI was mainly observed at tumor sites. The fluorescence intensity of Cy5-DM-AI in the tumor tissue decreased with time over 4 days post-injection (Fig. 6C).

The in vivo anticancer effects of DM-AI were studied using the dosing scheme illustrated in Fig. 7A. After primary tumor inoculation, the mice were intratumorally administered with the various microparticles. To test the importance of hIL2 entrapment inside DM-AI, the in vivo anticancer effects were evaluated for physical mixtures of PS-A with hIL2 or DM-A with hIL2. PS-A and PS-A + hIL2 reduced the tumor size by 4.6% and 24.1%, respectively; DM-A inhibited tumor growth by 60.1%; and DM-AI showed the highest in vivo anticancer effect, inhibiting CT26tumor growth by 98.7% over 27 days (Fig. 7B). On day 27 after tumor inoculation, no primary tumor could be detected in 80% of mice in the group treated with DM-AI (Fig. 7C).

In the group treated with DM-AI, the level of granzyme B in the tumor tissues was the highest (Fig. 7D). The population of CD8 and granzyme B-positive cells ($CD8^+GrzB^+$ cells) was significantly higher in the group treated with DM-AI compared to the other groups. The population of $CD8^+GrzB^+$ cells in the DM-AI-treated group was 1.4- and 2.0-fold higher than that in the groups treated with DM-A and PS-A, respectively (Fig. 7E).

The intratumoral injection of CT26 primary tumor tissues with DM-AI modulated the T cell subpopulations of the tumor microenvironment. The Treg cell population in tumor tissues was lowest in the group treated with DM-AI (Fig. 8A). The population of $CD4^+CD25^+FoxP3^+$ T cells in the DM-AI-treated group was 2.3- and 6.2-fold smaller than those of the groups treated with DM-A and PS-A, respectively (Fig. 8B). Although DM-AI significantly decreased the population of Treg cells in the tumor tissues, it significantly increased the population of $CD3^+CD8^+$ T cells compared with those found in the other groups (Fig. 8C). The co-

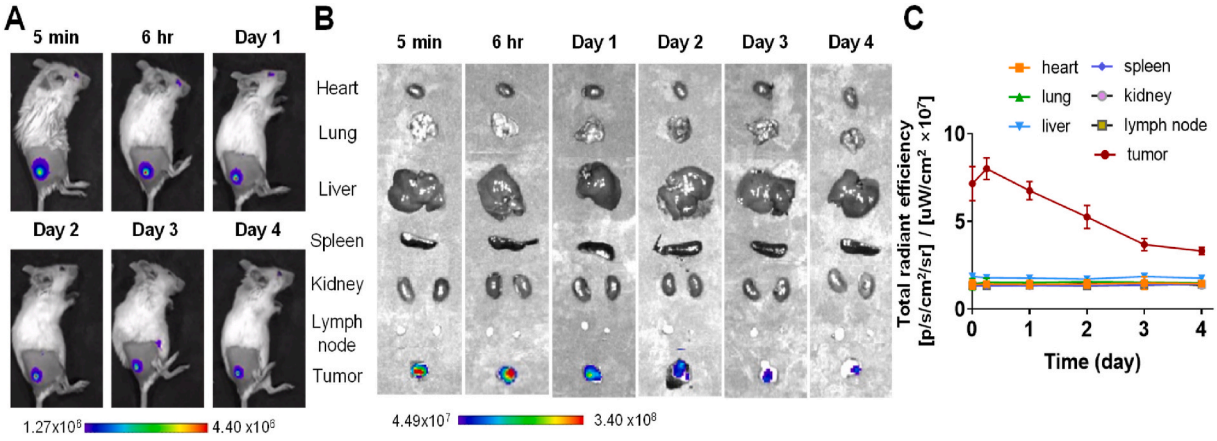

Fig. 6. Biodistribution of Cy5-DM-AI. Mice (n = 3) were subcutaneously inoculated with CT26 tumor cells and intratumorally injected with Cy5-DM-AI. (A) The fluorescence intensities of Cy5-DM-AI were monitored in the whole body using an IVIS Spectrum instrument equipped to monitor 651 nm excitation and 670 nm emission wavelengths. (B) At various time points, six vital organs (liver, heart, lung, spleen, kidney, and lymph node) and tumor tissues were extracted for ex vivo imaging. (C) Fluorescence intensities of ex vivo imaging were plotted with time.

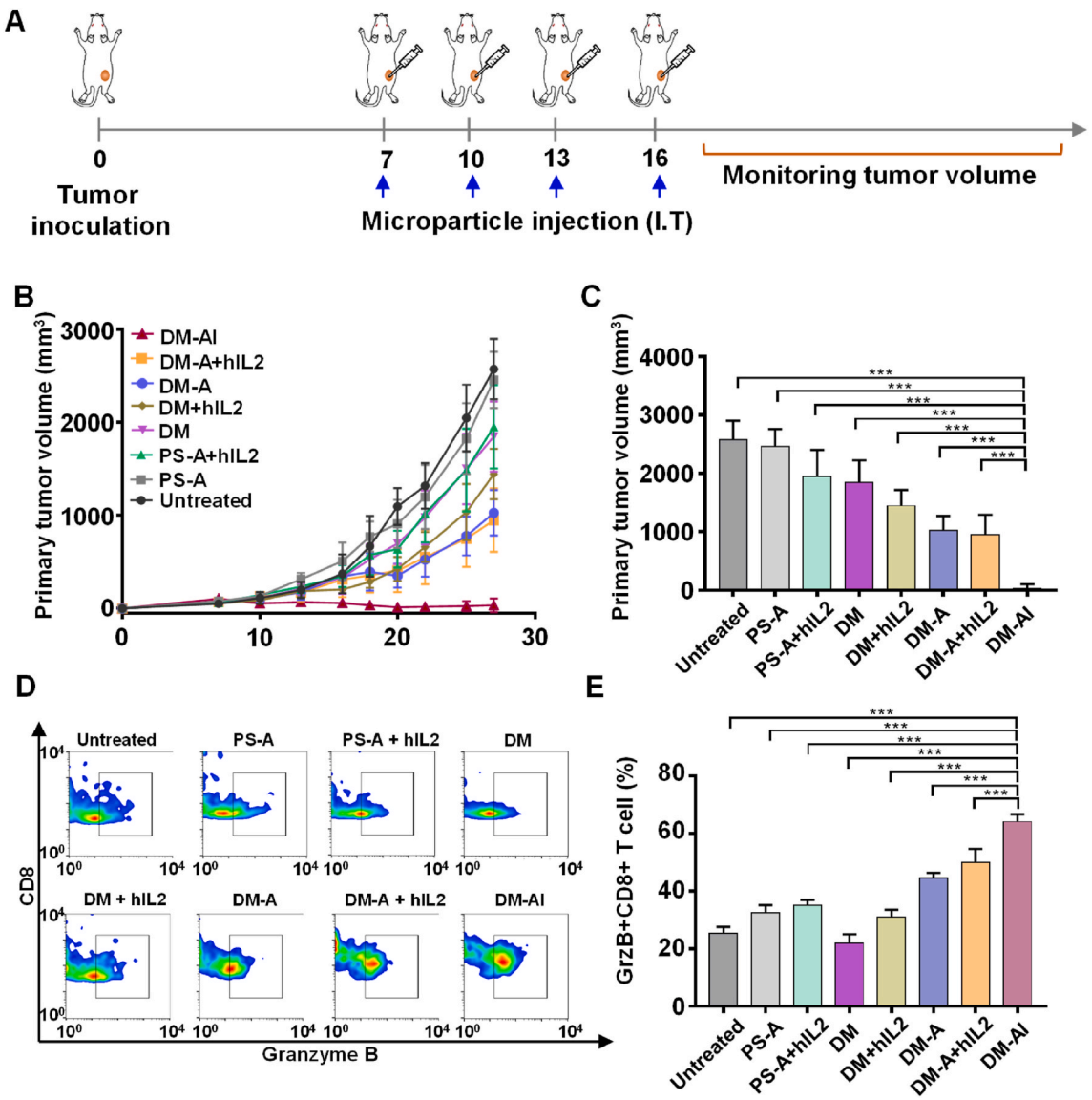

Fig. 7. In vivo antitumor effect of DM-AI. (A) Illustration of dosing schedule. Mice (n = 5) were subcutaneously inoculated with CT26 tumor cells and treated four times with the various samples. (B) Primary tumor volumes were monitored over 27 days. (C) Primary tumor volume at day 27 after primary tumor inoculation. (E, F) At day 7 after the first microparticle treatment, tumor tissues were analyzed as the percentage of granzyme B-expressing $CD8^+$ T cells, which was based on the gating of $GrzB^+CD8^+$ T cells (n = 3). ***: significantly different from the other groups at $P < 0.001$.

injection of DM-A plus hIL2 yielded 13.2 ± 1.9% $CD3^+CD8^+$ T cells, whereas DM-AI treatment yielded 23.7 ± 4.1% $CD3^+CD8^+$ T cells in tumor tissues (Fig. 8D).

3.6. Systemic immune responses induced by DM-AI

The systemic antitumor effect caused by local immunotherapy was evaluated by monitoring the growth of distant tumors (Fig. 9A). Co-treatment of PS, PS-A, DM, or DM-A with hIL2 did not completely prevent the growth of distant tumors. In contrast, the administration of DM-AI completely prevented the growth of distant CT26 tumors (Fig. 9B). Survival of mice was recorded at 70 days after tumor inoculation. Mice treated with PS-A, PS-A + hIL2, DM, or DM + hIL2 showed 0% survival. Among mice treated with DM-A and DM-A + hIL2, 20% survival was observed. Notably, all mice treated with DM-AI survived at least 70 days after the first inoculation of primary tumor cells (Fig. 9C and D).

Analysis of T cell populations in the distant tumor tissues showed that the highest infiltration of $CD8^+$ T cells was seen in mice treated with DM-AI (Fig. 9E). In distant tumor tissues, the population of $CD8^+$ T cells was 5.6- and 20.1-fold higher in the group treated with DM-AI versus the groups treated with DM-A and PS-A, respectively (Fig. 9F). Real-time video imaging showed that CT26 cells co-cultured with T cells from naïve mice remained viable and divided over time (Fig. 9G, supplementary Video S1A). In contrast, the co-culture of CT26 cells with T cells from the mice treated with DM-AI showed that tumor cells were attacked and killed by stimulated T cells (Fig. 9H, supplementary Video S1B).

Supplementary video related to this article can be found at https://doi.org/10.1016/j.bioactmat.2021.12.001

4. Discussion

We herein report that our newly constructed dendritic cell-mimetic DM-AI could stimulate T cells to proliferate to $CD8^+$ T cells and kill tumor cells ex vivo and in vivo. In addition, the treatment of mice with DM-AI prevented the growth of distant tumors and provided complete survival of the tumor cell-inoculated mice.

The immunotherapeutic effect of DM-AI reflects its close interaction

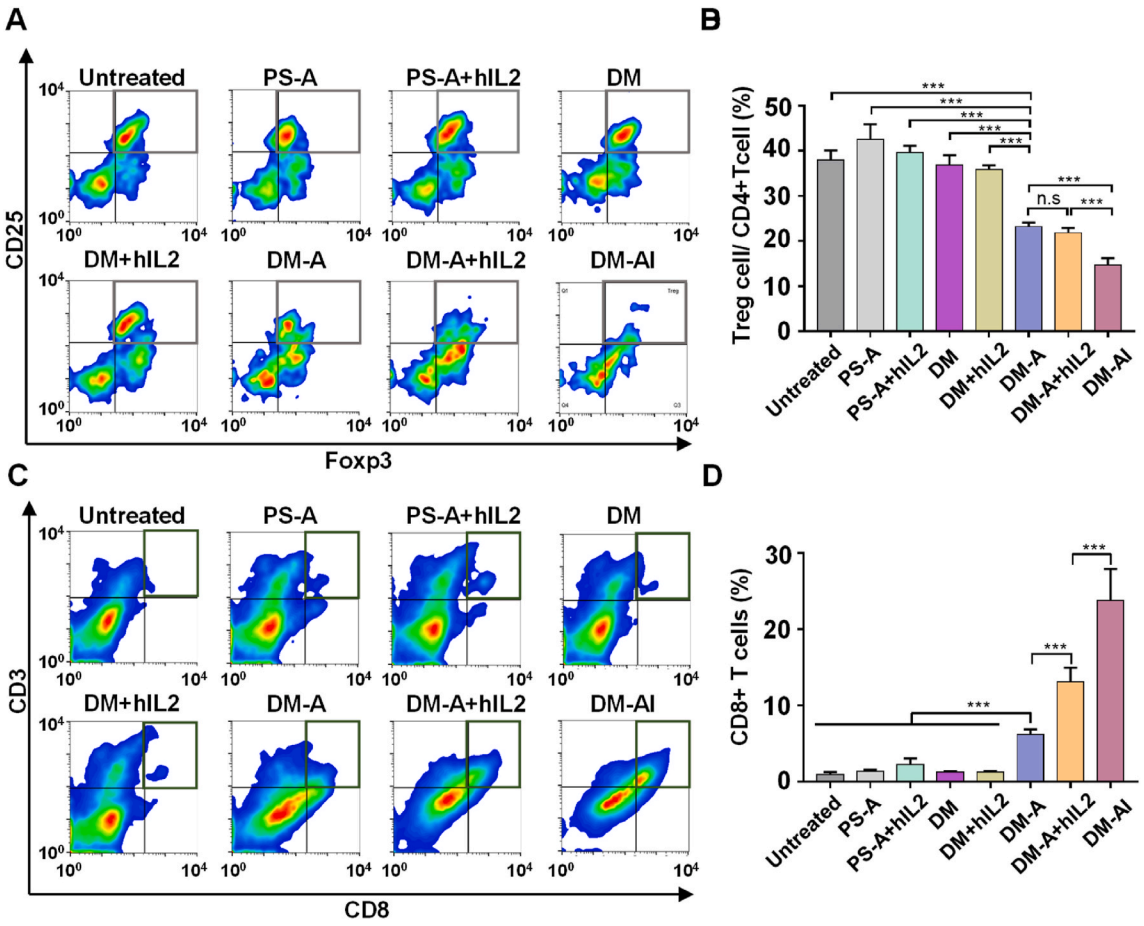

Fig. 8. Populations of T cells in primary tumor microenvironments. At day 7 after the first dosing with various microparticles, tumor tissues were analyzed for their T cell populations. (A, B) The percentage of Treg cells was based on the gating of $CD4^+CD25^+FoxP3^+$ T cells (n = 3). (C, D) The percentage of $CD8^+$ T cells in tumor tissues was analyzed by gating the $CD3^+CD8^+$ population in each group (n = 3). ***: significantly different from the other groups at $P < 0.001$.

with T cells, which mimics the close interaction of T cells and dendritic cells. The dendritic morphology of DM-AI was inspired by the microflower shape of RCA-amplified DNA products. In our previous studies, we observed that DNA-derived microflower shaped structures could be generated by RCA [14,15]. The microflower-like structure of DM-AI, with its multiple leaflets, may enable DM-AI to closely interact with T cells. Our results support the idea that the dendritic topology of DM-AI could increase its contact length with T cells, compared to that achieved using smooth microbeads, such as PS-A. Previous studies reported the importance of contact areas between T cells and T cell-stimulating microparticles, and found that the contact areas may play pivotal roles in the sequential activation of T cells [8,16].

DM-AI was designed to include anti-CD28 antibody, anti-CD3-antibody, and hIL2. Dendritic cells reportedly use three signals to activate T cells [5]: In the interaction between dendritic cells and T cells, the recognition of T cell receptor and CD3 complex by MHC on dendritic cells will stimulate T cells. To mimic this property of dendritic cells, we used anti-CD3 antibody to stimulate the non-specific clonal expansion of T cells [17], anti-CD28 antibody to potentially mimic the activation of T cells by CD80/86 co-stimulatory molecules [17], and hIL2 to possibly enhance these T cell-stimulating effects. In addition, IL2 has been reported to be crucial for the long-term survival of activated T cells [5,6]. Unlike PS-A, which had a solid hard core, DM-AI had a porous microstructure that provided spaces for the physical loading of hIL2.

To enable the generated particles to be surface-modified with T cell-stimulating antibodies, both DM and PS, which lack active functional groups for covalent conjugation with antibodies, were coated with PDA. This well-known coating material can adhere to diverse surfaces (hydrophilic, hydrophobic, etc.) [15] and may interact with DNA surfaces via hydrogen bonding and pi-pi stacking with the DNA backbone [18]. PDA-coated surfaces can be easily modified with various antibodies [11], and the presence of active catechol groups in PDA can allow antibodies to be conjugated at mildly basic pH conditions [19].

The microflower-like structure of DM-AI provided a larger surface area than that of the spherical PS. The different topology of DM might have contributed to the higher amounts of antibodies that underwent surface binding Notably, in both DM and PS, loading was higher for the anti-CD28 antibody than for the anti-CD3 antibody. This was due to the ratio of antibodies in the reaction mixture. As the binding ratio reflected the ratio of the physical mixture, our results suggest that the antibody type did not affect the binding efficacy to DM or PS.

In our ex vivo study, we observed that DM-AI could support the expansion of T cells to $CD8^+$ T cells with relatively little expansion to Treg cells. The preferential stimulation to $CD8^+$ T cells may explain the higher tumor killing effects observed for this formulation. Several studies found a correlation between a positive clinical outcome of cancer patients and a high $CD8^+$ T cell/Treg cell ratio [2,3]. The higher $CD8^+$ T cell/Treg ratio observed in our ex vivo study might be due to the increased interaction of T cells with DM-AI. The release of hIL2 from DM-AI could also contribute to $CD8^+$ T cell stimulation. Several studies have reported that IL2 released from particles could promote the proliferation of $CD8^+$ T cells more actively than free IL2 [7,20].

To date, various nanomaterials have been investigated for the development of artificial dendritic cells. Iron oxide microparticles [21], poly lactic-*co*-glycolic acid (PLGA) microparticles [22], liposome [23], and polymeric string-based nanoworms [24] have been reported. Iron

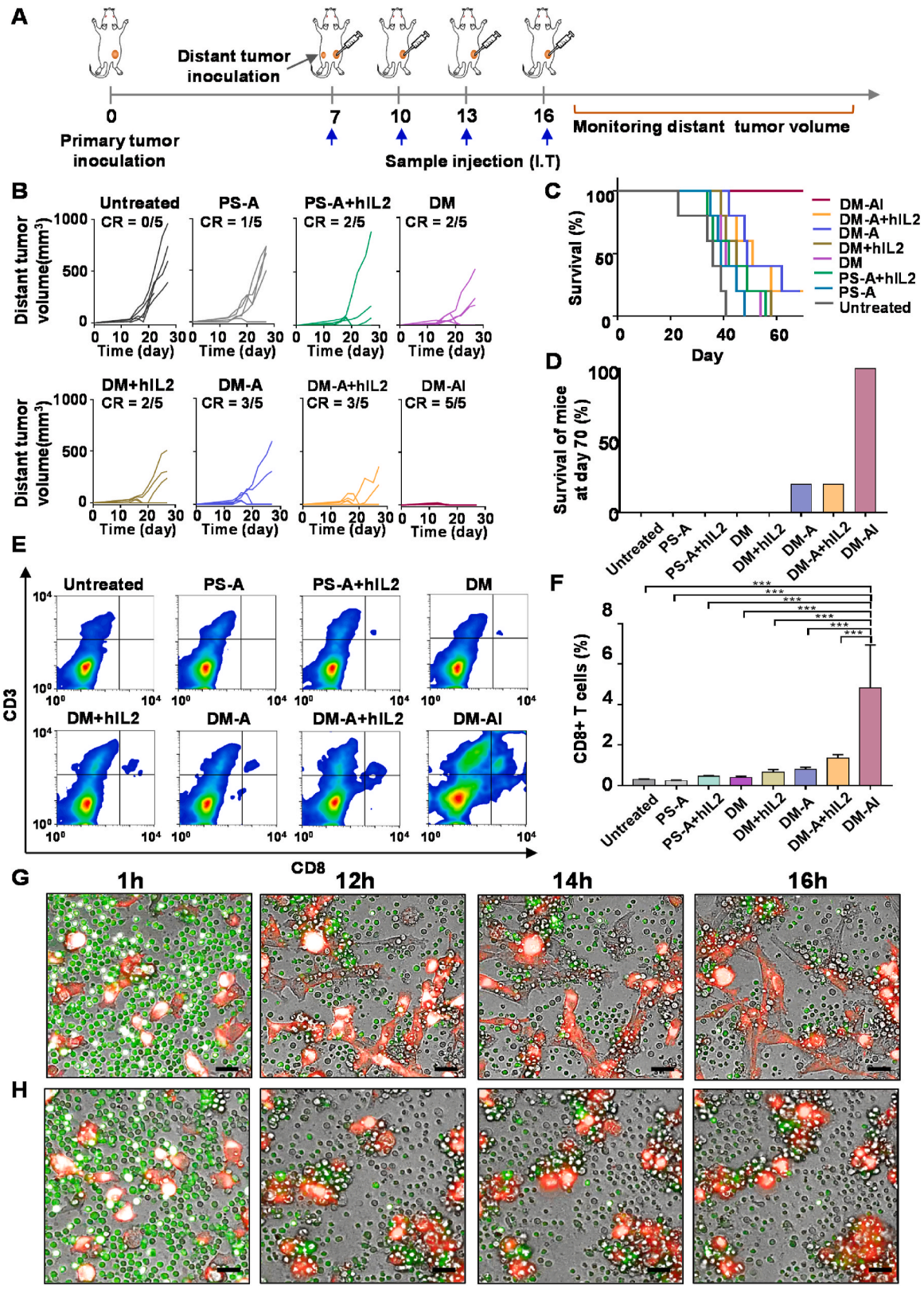

Fig. 9. Systemic immune responses by DM-AI.
(A) Mice were inoculated with CT26 cells, and rechallenged with the same cells at day 7. Mice were locally injected with microparticles, as indicated (n = 5). (B) Distant tumor volumes were measured for each group (n = 5). (C) Survival of mice was monitored over 64 days after the primary tumor cell inoculation. (D) Survival of mice was recorded at day 70 after tumor inoculation (n = 5/group). (E, F) Percentage of $CD8^+$ T cells in distant tumor tissues at day 7 after distant tumor inoculation (n = 5). (G, H) T cells derived from splenocytes of naïve mice (G) or DM-AI-treated mice (H) were co-cultured with CT26 cells. Scale bar: 30 μm. Time-lapse video images are presented. Video files are provided as Supplementary Video S1. ***: significantly different at $P < 0.001$.

oxide microbeads were one of the earliest artificial dendritic cells, reflecting their facile synthesis process and the simplicity of scaling up. However, iron oxide microparticles suffer from a lack of biodegradability, limiting their application for human use. Unlike iron oxide microparticles, PLGA microbeads have the advantage of biodegradability. However, similar to PS microparticles, PLGA microbeads have smooth surfaces with limited surface contact area for T cells. To increase the contact area with T cells, researchers studied an ellipsoidal PLGA bead [25]. Although there has been progress in efforts to change the morphology with synthetic polymers, the available shape-controlling techniques remain complicated.

Liposome and polymeric nanoworms have been investigated as T cell activators for proper engagement of receptors on T cell surfaces [24]. Either liposomes or polymeric string-based nanoworms have little capacity to encapsulate or entrap macromolecular cytokines. Unlike these nanomaterials, DM-AI comprises a DNA backbone, and thus features biodegradability for clinical use. In addition, the unique microflower-shaped topology offers a large contact area and a porous structure for internal cytokine entrapment. In addition, the PDA coating layer of DM-AI enables further chemical modification with antibodies and provides the potential for photoimmunotherapy in combination with a light stimulus.

Although we used DM-AI for cancer immunotherapy as a proof-of-concept, the design of DM-AI can be widely applied for treating other immunological diseases. Here, for cancer immunotherapy requiring the activation of $CD8^+$ T cells in the tumor immune microenvironment, we used anti-CD3 antibody, anti-CD28 antibody, and hIL2. However, the modification of DM with other antibodies and cytokines could be used to modulate the propagation of T cells in other directions. For example, the modification of particles with antibody plus immunosuppressive signals might generate a formulation that triggers expansion of T cells against autoimmune diseases.

5. Conclusion

In summary, we took advantage the unique surface topology of DNA-microflowers to develop a novel platform for T cell activation. The large surface area of DM-AI increased the interaction with T cells, resulting in higher stimulation of T cells. The biodegradable and biocompatible features of the DNA-based matrix should contribute to the safety of this formulation in future translational studies. Here, we describe DM-AI with hIL2 and two antibodies for directing T cell expansion. By changing the cytokine and antibodies, this concept can be applied to direct the expansion of different cells for cell therapy and immunotherapy.

CRediT authorship contribution statement

Quoc-Viet Le: Conceptualization, Methodology. **Jaiwoo Lee:** Conceptualization, Methodology. **Junho Byun:** Data curation, Visualization. **Gayong Shim:** Data curation, Investigation, Writing – original draft, Preparation. **Yu-Kyoung Oh:** Writing – review & editing, Supervision.

Declaration of competing interest

The authors declare no potential conflicts of interest.

Acknowledgements

This research was supported by grants from the Basic Science Research Program through the National Research Foundation of Korea (NRF) funded by the Ministry of Science and ICT, Republic of Korea (NRF-2021R1A2B5B03002123; NRF-2018R1A5A2024425), the Ministry of Education (NRF-2020R1I1A1A01070084; NRF-2020R1A6A3A01099750), the Korean Health Technology R&D Project (No. HI18C2177), Ministry of Health & Welfare, and a Korea Medical Device Development Fund grant funded by the Korean government (the Ministry of Science and ICT, the Ministry of Trade, Industry and Energy, the Ministry of Health & Welfare, the Ministry of Food and Drug Safety) (Project Number: 9991007273, KMDF_PR_20200901_0106), Republic of Korea.

Appendix A. Supplementary data

Supplementary data to this article can be found online at https://doi.org/10.1016/j.bioactmat.2021.12.001.

References

[1] A.D. Waldman, J.M. Fritz, M.J. Lenardo, A guide to cancer immunotherapy: from T cell basic science to clinical practice, Nat. Rev. Immunol. 20 (11) (2020) 651–668.
[2] J. Wang, S. Tian, J. Sun, J. Zhang, L. Lin, C. Hu, The presence of tumour-infiltrating lymphocytes (TILs) and the ratios between different subsets serve as prognostic factors in advanced hypopharyngeal squamous cell carcinoma, BMC Cancer 20 (2020) 1–12.
[3] W. Yao, J.C. He, Y. Yang, J.M. Wang, Y.W. Qian, T. Yang, L. Ji, The prognostic value of tumor-infiltrating lymphocytes in hepatocellular carcinoma: a systematic review and meta-analysis, Sci. Rep. 7 (1) (2017) 1–11.
[4] R. Saleh, E. Elkord, FoxP3+ T regulatory cells in cancer: prognostic biomarkers and therapeutic targets, Cancer Lett. 490 (2020) 174–185.
[5] J.C. Sunshine, J.J. Green, Nanoengineering approaches to the design of artificial antigen-presenting cells, Nanomedicine 8 (7) (2013) 1173–1189.
[6] K.R. Rhodes, J.J. Green, Nanoscale artificial antigen presenting cells for cancer immunotherapy, Mol. Immunol. 98 (2018) 13–18.
[7] E.R. Steenblock, T. Fadel, M. Labowsky, J.S. Pober, T.M. Fahmy, An artificial antigen-presenting cell with paracrine delivery of IL-2 impacts the magnitude and direction of the T cell response, J. Biol. Chem. 286 (40) (2011) 34883–34892.
[8] J.C. Sunshine, K. Perica, J.P. Schneck, J.J. Green, Particle shape dependence of $CD8^+$ T cell activation by artificial antigen presenting cells, Biomaterials 35 (1) (2014) 269–277.
[9] L. Zhang, S. Song, X. Jin, X. Wan, K.A. Shahzad, W. Pei, C. Zhao, C. Shen, An artificial antigen-presenting cell delivering 11 immune molecules expands tumor antigen–specific CTLs in ex vivo and in vivo murine melanoma models, Cancer Immunol Res 7 (7) (2019) 1188–1201.
[10] E. Ben-Akiva, K.R. Rhodes, R.A. Meyer, J.J. Green, Fabrication of anisotropic polymeric artificial antigen presenting cells for $CD8^+$ T cell activation, JoVE: JoVE (140) (2018) 58332.
[11] Q.V. Le, J. Suh, J.J. Choi, G.T. Park, J.W. Lee, G. Shim, Y.K. Oh, In situ nanoadjuvant-assembled tumor vaccine for preventing long-term recurrence, ACS Nano 13 (7) (2019) 7442–7462.
[12] P.D. Sciullo, F. Menay, F. Cocozza, M.J. Gravisaco, C.I. Waldner, C. Mongini, Systemic administration of imiquimod as an adjuvant improves immunogenicity of a tumor-lysate vaccine inducing the rejection of a highly aggressive T-cell lymphoma, Clin. Immunol. 203 (2019) 154–161.
[13] Y. Wu, Q. Li, G. Shim, Y.K. Oh, Melanin-loaded CpG DNA hydrogel for modulation of tumor immune microenvironment, J. Control Release 330 (2021) 540–553.
[14] E. Kim, L. Zwi-Dantsis, N. Reznikov, C.S. Hansel, S. Agarwal, M.M. Stevens, One-pot synthesis of multiple protein-encapsulated DNA flowers and their application in intracellular protein delivery, Adv. Mater. 29 (26) (2017) 1701086.
[15] G. Shim, J. Park, M.G. Kim, G. Yang, Y. Lee, Y.K. Oh, Noncovalent tethering of nucleic acid aptamer on DNA nanostructure for targeted photo/chemo/gene therapies, Nanomedicine 24 (2020) 102053.
[16] J.W. Hickey, F.P. Vicente, G.P. Howard, H.-Q. Mao, J.P. Schneck, Biologically inspired design of nanoparticle artificial antigen-presenting cells for immunomodulation, Nano Lett. 17 (11) (2017) 7045–7054.
[17] L.J. Eggermont, L.E. Paulis, J. Tel, C.G. Figdor, Towards efficient cancer immunotherapy: advances in developing artificial antigen-presenting cells, Trends Biotechnol. 32 (9) (2014) 456–465.
[18] W.-R. Zhuang, Y. Wang, P.-F. Cui, L. Xing, J. Lee, D. Kim, H.-L. Jiang, Y.-K. Oh, Applications of π-π stacking interactions in the design of drug-delivery systems, J. Contr. Release 294 (2019) 311–326.
[19] Y. Liu, K. Ai, L. Lu, Polydopamine and its derivative materials: synthesis and promising applications in energy, environmental, and biomedical fields, Chem. Rev. 114 (9) (2014) 5057–5115.
[20] A.S. Cheung, D.K. Zhang, S.T. Koshy, D.J. Mooney, Scaffolds that mimic antigen-presenting cells enable ex vivo expansion of primary T cells, Nat. Biotechnol. 36 (2) (2018) 160.
[21] Y. Li, R.J. Kurlander, Comparison of anti-CD3 and anti-CD28-coated beads with soluble anti-CD3 for expanding human T cells: differing impact on CD8 T cell phenotype and responsiveness to restimulation, J. Transl. Med. 8 (2010) 104.
[22] E.R. Steenblock, T.M. Fahmy, A comprehensive platform for ex vivo T-cell expansion based on biodegradable polymeric artificial antigen-presenting cells, Mol. Ther. 16 (4) (2008) 765–772.
[23] R. Zappasodi, M. Nicola, C. Carlo-Stella, R. Mortarini, A. Molla, C. Vegetti, S. Albani, A. Anichini, A.M. Gianni, The effect of artificial antigen-presenting cells with preclustered anti-CD28/-CD3/-LFA-1 monoclonal antibodies on the induction

of ex vivo expansion of functional human antitumor T cells, Haematologica 93 (10) (2008) 1523–1534.

[24] S. Mandal, Z.H. Eksteen-Akeroyd, M.J. Jacobs, R. Hammink, M. Koepf, A. J. Lambeck, J.C.M. van Hest, C.J. Wilson, K. Blank, C.G. Figdor, A.E. Rowan, Therapeutic nanoworms: towards novel synthetic dendritic cells for immunotherapy, Chem. Sci. 4 (11) (2013) 4168–4174.

[25] J.C. Sunshine, K. Perica, J.P. Schneck, J.J. Green, Particle shape dependence of $CD8^+$ T cell activation by artificial antigen presenting cells, Biomaterials 35 (1) (2014) 269–277.